Negative conductance patterns of quantum dots: experiment and theory

2006 New J. Phys. 8 298

(http://iopscience.iop.org/1367-2630/8/12/298)

New Journal of Physics
The open–access journal for physics

Negative conductance patterns of quantum dots: experiment and theory

M C Rogge[1], F Cavaliere[2,3], M Sassetti[3], R J Haug[1], B Kramer[2,4]

[1] Institut für Festkörperphysik, Universität Hannover, Appelstraße 2, 30167 Hannover, Germany
[2] Institut für Theoretische Physik, Universität Hamburg, Jungiusstraße 9, 20355 Hamburg, Germany
[3] INFM-CNR Lamia, Dipartimento di Fisica Università di Genova, Via Dodecaneso 33, 16146 Genova, Italy
[4] International University Bremen, Campus Ring 1, 28759 Bremen, Germany
E-mail: rogge@nano.uni-hannover.de

New Journal of Physics **8** (2006) 298
Received 28 September 2006
Published 1 December 2006
Online at http://www.njp.org/
doi:10.1088/1367-2630/8/12/298

Abstract. Experimental results for the sequential transport through a lateral quantum dot in a perpendicular magnetic field are compared with theory. Regular patterns of negative differential conductances are observed in the nonlinear regime. We attempt to reproduce theoretically these patterns in a simplified model which captures the essential features of the experimental system. Orbital and spin effects are treated in terms of the Fock–Darwin model. The transport properties are described by employing a master equation with tunable tunnelling and relaxation rates. We show that the essential physics underlying the experiment can be described within our approach if the timescales of the different transport channels are well separated.

PII: S1367-2630(06)30561-7

Contents

1. Introduction

Since the discovery of the Coulomb blockade effect in semiconductors [1] electronic transport properties of lateral quantum dots have been the subject of continuous interest [2]. The interplay of Coulomb interaction, the spectra of orbital states and the electron spin, causes a rich variety of effects in the transport spectra [3]. In a high external magnetic field, signatures have been found for transitions between different angular momentum states of the single electron Fock–Darwin spectrum [4], modified by interactions [5]. Effects of the electron spin have been observed, including spin blockade. The latter was experimentally found in split gate quantum dots and assigned to spin polarization of the leads which implies spin dependent amplitudes of Coulomb peaks [6, 7]. Recently, this has also been observed in devices made with local anodic oxidation (LAO) [8]. In nonlinear transport, negative differential conductance (NDC) was found and explained in terms of spin dependent tunnelling [9].

Theoretically, transport in multi-level quantum dots within the sequential tunnelling regime employing master equation techniques has been the subject of investigations both in the linear and in the nonlinear regime [10]–[14]. Another type of spin blockade, leading to NDC in the nonlinear transport regime has been theoretically predicted as a consequence of spin selection rules in multilevel quantum dots [15]. More recently, weak violations to that type of spin blockade, caused by spin relaxation, have been analysed [16]. NDC has been predicted to occur also as a result of electron correlations beyond the classical Coulomb interaction, leading to a dynamical trapping of the excited states in the quantum dot [17].

In this paper, we report experimental results on the nonlinear conductance spectra of a quantum dot in a GaAs/AlGaAs heterostructure, studied as a function of a perpendicular magnetic field in the sequential tunnelling regime. An attempt is made to theoretically understand the results by using, as a starting point, the Fock–Darwin single particle spectrum. The presence of interaction is taken into account including a constant interaction Coulomb energy. In addition, within a semi-phenomenological approach, the rates will be considered as tunable parameters. They will be determined by reproducing the experimental data. We find a specific hierarchy

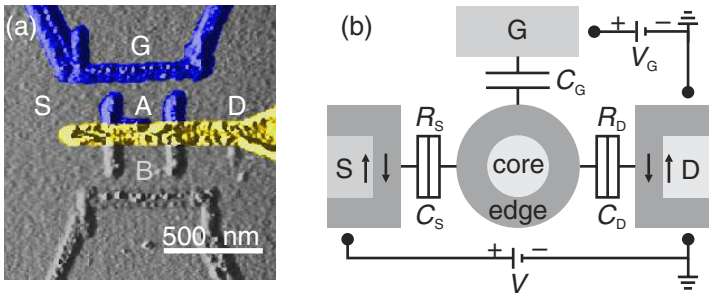

Figure 1. (a) AFM picture of the gate structures used to define electrostatically a lateral quantum dot in the inversion layer of a GaAs/AlGaAs heterostructure. (b) Electrostatic model for the device in a perpendicular magnetic field. The dot is coupled via tunnel resistances $R_{S,D}$ and capacitances $C_{S,D}$ to source S and drain D that feature spin split edge channels. The in-plane gate G is capacitively coupled.

among rates with a separation of the different timescales associated to transport processes. An intuitive understanding of the physical processes responsible for the results is developed.

The paper is organized as follows. The experimental setup and the results for the differential conductance in the linear and nonlinear regimes are described in section 2. In section 3, the theoretical model is discussed. The fundamental features of the single-particle spectrum are described, the master equation, the tunnelling and the relaxation rates are introduced. The comparison between experiments and theory is presented in section 4.

2. Experiment

The quantum dot has been fabricated in an inversion layer of a GaAs-heterostructure. The two-dimensional (2D) electron system is located 34 nm below the surface. The sheet density is $n = 4.3 \times 10^{15}\,\mathrm{m}^{-2}$. A combination of LAO with an atomic force microscope and electron beam lithography is used to define the quantum dot in figure 1(a). Details of the sample processing can be found in [18, 19]. Dot A is coupled to source (S) and drain (D) leads via resistances R_S and R_D, with capacitances C_S and C_D (figure 1(b)). An in-plane gate G is capacitively coupled via C_G and can be biased to tune the electron number n in the dot. The experiments are performed in a regime where dot B, which is coupled capacitively to dot A, is only connected to the source and completely disconnected on the drain side [8]—thus transport occurs only via dot A (from now on called 'the dot'). The differential conductance is recorded using standard lock-in techniques at temperature $T = 50\,\mathrm{mK}$, where the dot is in the Coulomb blockade regime.

Figure 2 shows experimental results of the differential conductance as a function of gate voltage V_G and magnetic field B. In the linear regime with no dc-voltage applied to the leads, figures 2(a) and (b), sawtooth-like traces reflecting ground state transitions become visible (blue features). The peak positions of these traces show a periodical behaviour as does the peak amplitude. The sawtooth-like traces are very weak for positive slopes, and show a 'bimodal' pattern of strong–weak intensities for lines with negative slopes. In addition for fixed B, neighbouring Coulomb peaks are shifted by half a period thus exhibiting a periodic pattern of strong and weak conductances when increasing V_G [6, 20]. In the nonlinear regime with

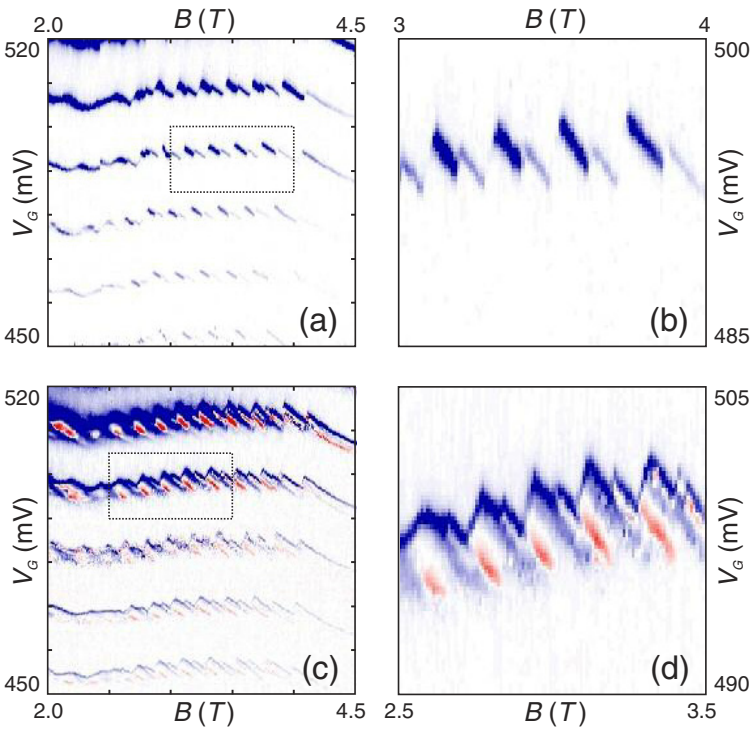

Figure 2. (a) Positions of linear conductance peaks of the dot in the plane of gate voltage V_G and magnetic field B (dark: high conductance, bright: low conductance); (b) zoom of (a). (c) Spectrum of the nonlinear conductance peaks at bias $V = 0.5\,\mathrm{mV}$, red: NDC; (d) zoom of (c). Regular patterns of PDC and NDC are observed with absent transitions with positive slopes.

a finite voltage applied to the leads, figures 2(c) and (d), apart from the ground-state transition (upper sawtooth-like trace in figure 2(d)), traces due to excited states are found below the ground-state trace. For those excited states conductance lines with positive slopes are *absent* and only lines with *negative* slopes are observed with a distinct bimodal pattern of positive (PDC, blue) and NDC (red). In the nonlinear regime, the ground-state transition is actually split into two transitions with one trace expected below the excited states. Due to asymmetry of source and drain capacitances, $C_S \ll C_D$, lines corresponding to transitions $n \to n + 1$ (cf figures 2(c) and (d)) have vanishing intensities leaving only the upper traces visible.

3. Theory

The experimental results are presented in a range of magnetic field with filling factor $2 < \nu < 4$. In the following, the theoretical model will describe this regime.

3.1. Model for the quantum dot

We model the Hamiltonian for n electrons in the quantum dot, with perpendicular magnetic field B, as $H_d = H_0 + H_1$. The first term is a single particle contribution ($\hbar = 1$)

$$H_0 = \sum_{i=1}^{n} \varepsilon_{\beta_i} |\beta_i\rangle\langle\beta_i|, \tag{1}$$

where we employ the Fock–Darwin spectrum [4]. States are denoted by $|\beta\rangle = |q, l, \sigma\rangle$, with energy

$$\varepsilon_{q,l,\sigma} = \Omega\,(2q+1) - \left(\Omega - \frac{\omega_c}{2}\right) l + \sigma g^* \mu_B B. \tag{2}$$

Here, we consider only the two lowest Landau levels (LL), represented by $q = 0$ and $q = 1$, each with two spin branches up (down) identified by $\sigma = +$ ($\sigma = -$). Within a given LL, different states are further represented by the angular momentum l with[5] $-\infty < l \leqslant q$, at finite magnetic fields they are not degenerate in energy. At fixed q and l the states are also spin–split, because of the Zeeman term (last term in equation (2)). We consider the value for GaAs, $g^* = -0.44$. The cyclotron frequency is $\omega_c = eB/m^*$ (e, m^* electron charge and effective mass) and

$$\Omega = [\omega_0^2 + (\omega_c/2)^2]^{1/2} \tag{3}$$

represents the effective quantum dot confinement, ω_0 being the bare confinement frequency at zero field.

A plot of the above Fock–Darwin spectrum as a function of B is depicted in figure 3(a). Levels with $q = 0$ ($q = 1$) are plotted with red (black) lines. Solid (dashed) lines represent $\sigma = -(\sigma = +)$. The bold blue line shows the energy of the nth electron. It has a sawtooth shape, with positive (negative) slope corresponding to states in LL $q = 1$ ($q = 0$). Because of the Zeeman splitting, levels with opposite spins alternate. In figure 3(b), a zoom of the spectrum around $\nu = 2$ is shown. For simplicity, only levels with $\sigma = -$ are considered. States with $q = 0, 1$ are shown together with their angular momentum l. It can be seen that states with $q = 0$ (red) have angular momenta *higher in absolute value* than the corresponding state with $q = 1$ (black). This discrepancy in l occurs in the whole $2 < \nu < 4$ range and results in a spatial separation of the wavefunctions with $q = 0$ and $q = 1$: wavefunctions with $q = 0$ are more peaked towards the border of the dot, while those with $q = 1$ are more peaked near to the centre. For this reason, we will refer to states with $q = 0$ as 'edge states' while states with $q = 1$ will be called 'core states' [5, 21].

The Coulomb interaction is described by a constant charging energy E_c

$$H_1 = \frac{E_c}{2} n^2 - \frac{en}{C_\Sigma}(V_G C_G + V C_S). \tag{4}$$

The gate voltage V_G tunes the effective charge on the quantum dot, while the term proportional to V stems from the coupling to the external bias voltage.

[5] Note that in order to occupy the lowest two LL only, the possible angular momenta in a given LL are constrained to $-|l_{min}| < l \leqslant q$, with l_{min} depending on the magnetic field and the number of particles. For $l < -|l_{min}|$ higher LLs enter in the energy spectrum.

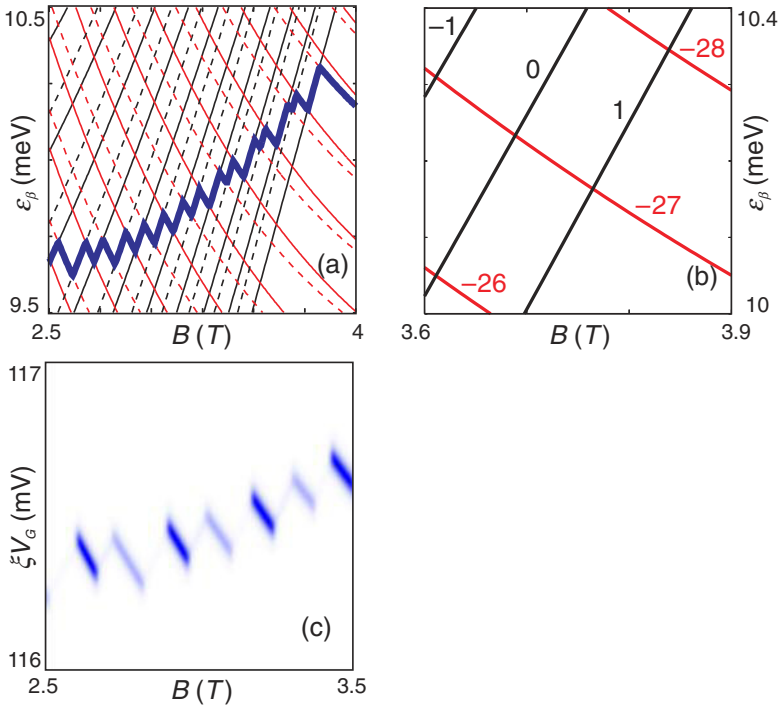

Figure 3. (a) Energy spectrum ε_β as a function of B for $2 < \nu < 4$. Red (black) lines: states with $q = 0$ ($q = 1$). Solid (dashed) lines: spin down (spin up) states. Bold blue: nth electron energy level; (b) zoom of (a) and corresponding angular momenta for states with $q = 0$ and $q = 1$ (colour code as above). For simplicity, only states $\sigma = -$ are depicted here; (c) calculated linear conductance trace as a function of V_G and B for transitions $n \leftrightarrow n + 1$ with $A_s = 0.3$ and $A_{gg}(1) = A_s/5$ (see text); other parameters: $\omega_0 = 1.3$ meV, $n = 56$, $T = 70$ mK ($\xi = C_G/C_\Sigma$).

3.2. Sequential tunnelling

The dot is connected to noninteracting leads via the tunnelling Hamiltonian

$$H_t = \sum_\lambda \sum_{k,q,l,\sigma} t^\lambda_{kql\sigma} d^\dagger_{ql\sigma} c^\lambda_{k\sigma} + \text{h.c.}, \tag{5}$$

with $d_{ql\sigma}$ and $c^\lambda_{k\sigma}$ dot and leads operators, respectively ($\lambda = S, D$ barrier index, k lead wavenumber). The tunnelling amplitudes are dominated by the overlap of the dot core/edge states and the leads wavefunctions, $t^\lambda_{kql\sigma} \approx t^\lambda_{q\sigma}$. In view of the considerations about the different spatial extensions of core and edge states, we expect $|t^\lambda_{1\sigma}| < |t^\lambda_{0\sigma}|$. In the leads, states with opposite spins are spatially separated at high magnetic field [6], thus within each LL one has $|t^\lambda_{q+}| < |t^\lambda_{q-}|$.

In order to describe the transport properties, we employ a master equation approach in the sequential regime, restricted to two charge states n and $n + 1$, tuned by the gate voltage. This implies a charging energy large with respect to temperature. Moreover, we consider only the three lowest-energy transitions, namely the transition between the two ground states $g_n \leftrightarrow g_{n+1}$, and the transitions between a ground state and the first excited state, $g_n \leftrightarrow e_{n+1}$ and $g_{n+1} \leftrightarrow e_n$.

This is a good approximation for external voltages and temperatures smaller than the average level separation. The master equation thus reads

$$\sum_{\alpha',\lambda}(P_\alpha \Gamma^{\lambda}_{\alpha\alpha'} - P_{\alpha'}\Gamma^{\lambda}_{\alpha'\alpha}) = 0, \tag{6}$$

with $\alpha, \alpha' \in \{g_n, g_{n+1}, e_n, e_{n+1}\}$. A dot state is expressed by $|\alpha\rangle = |n_\alpha, \{\beta\}\rangle$, where $n_\alpha = n, n+1$ and $\{\beta\}$ are the set of states occupied by the n_α electrons. The rate for the transition $\alpha \to \alpha'$ is

$$\Gamma^{\lambda}_{\alpha\alpha'}(\Delta E) = \Gamma^{t\lambda}_{\alpha\alpha'}(\Delta E)\delta_{n_{\alpha'},n_\alpha\pm1} + \gamma^{r}_{\alpha\alpha'}(\Delta E)\delta_{n_{\alpha'},n_\alpha}, \tag{7}$$

with $\Delta E = E_{\alpha'} - E_\alpha$ the exchanged energy. The tunnelling rates $\Gamma^{t\lambda}_{\alpha\alpha'}(\Delta E)$ connect states with different particle numbers. The relaxation rates $\gamma^{r}_{\alpha\alpha'}(\Delta E)$ (α or α' excited states) connect states with the same particle numbers. Several scattering processes can cause relaxation in a quantum dot [22]. Here, we consider a relaxation rate with a power law behaviour driven by the exponent η

$$\gamma^{r}_{\alpha\alpha'}(\Delta E) = \gamma^{r}(|\Delta E|/\omega_0)^{\eta} \qquad (\Delta E < 0), \tag{8}$$

$$\gamma^{r}_{\alpha\alpha'}(\Delta E) = \gamma^{r}(|\Delta E|/\omega_0)^{\eta}\, \mathrm{e}^{-\Delta E/k_\mathrm{B}T} (\Delta E \geqslant 0). \tag{9}$$

Note the presence of the Boltzmann factor to satisfy the detailed balance.

In the absence of interactions, the tunnelling rates are parameterized by the quantum numbers β of the electron entering or leaving the dot, $\Gamma^{t\lambda}_{\alpha\alpha'}(\Delta E) = \gamma^{\lambda}_{\alpha\alpha'}(\beta)\rho_\lambda f(\Delta E)$, with $f(\Delta E)$ and ρ_λ the Fermi function and density of states of the leads. These quantum numbers are uniquely determined by the overlap matrix elements $M_{\alpha\alpha'}(\beta) = \langle\alpha'|d^{\dagger}_{\beta}|\alpha\rangle$. Together with the tunnelling matrix elements, these define the rates $\gamma^{\lambda}_{\alpha\alpha'}(\beta) = |t^{\lambda}_{\beta}M_{\alpha\alpha'}(\beta) + [t^{\lambda}_{\beta}M_{\alpha'\alpha}(\beta)]^*|^2$. Varying B for a fixed transition $\alpha \to \alpha'$ implies changing β, which oscillates between $q = 0, 1$ and $\sigma = \pm$.

In the presence of interactions the electron states are superpositions of many Slater determinants of noninteracting states. This implies that $M_{\alpha\alpha'}(\beta)$ consists of many contributions of overlap matrix elements between Slater determinants and is in general renormalized as compared to the non-interacting limit. In order to describe phenomenologically these effects, we will consider tunable matrix elements $M_{\alpha\alpha'}(\beta)$, whose value will be determined *a posteriori* by comparison with the experiments. For a given state β, the matrix $M_{\alpha\alpha'}(\beta)$ mainly depends on value of the LL q, we then neglect the dependence on the angular momentum l. We further consider the case with $|M_{ge}(q)| = |M_{eg}(q)|$. The three possible transitions, are labelled by four combinations of $q = 0, 1$ and $\sigma = \pm$ which are selected by the magnetic field. This yields a total of 12 tunnelling rates per barrier.

We describe the hierarchy of the rates by defining six ratios per spin direction

$$A_{\alpha\alpha'}(q) = \frac{\gamma^{\lambda}_{\alpha\alpha'}(q,\sigma)}{\gamma^{\lambda}_{gg}(0,\sigma)}. \tag{10}$$

We also introduce three adimensional rates

$$A_\mathrm{s} = \frac{\gamma^{\lambda}_{gg}(0,+)}{\gamma^{\lambda}_{gg}(0,-)}, \qquad A_\mathrm{r} = \frac{\gamma^{r}}{\gamma^{D}_{gg}(0,-)}, \qquad A = \frac{\gamma^{S}_{\alpha\alpha'}(\beta)}{\gamma^{D}_{\alpha\alpha'}(\beta)} = \frac{R_\mathrm{D}}{R_\mathrm{S}}. \tag{11}$$

Here, A_s specifies rates with different spin orientations, A_r the relaxation rate and A the barrier asymmetry. Note that all the rates are expressed in units of $\gamma^{D}_{gg}(0,-)$. There are now eight independent parameters including η (see equation (8)) and the unit $\gamma^{D}_{gg}(0,-)$.

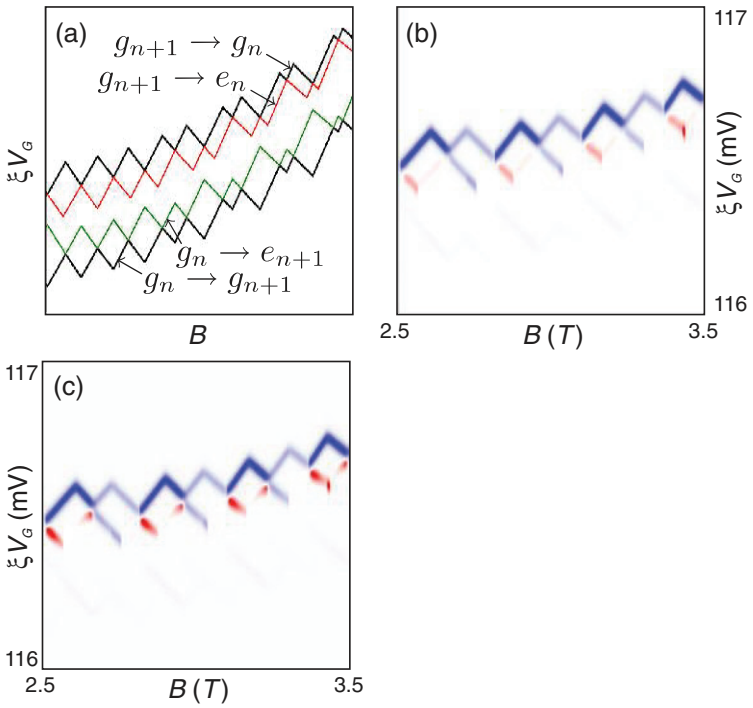

Figure 4. (a) Scheme of nonlinear conductance traces in the (B, V_G)-plane; (b) calculated nonlinear conductance for $A_s = 0.3$, $A_{gg}(1) = A_s/5$, $A_{ge}(1) = A_{gg}(1)/9$, $A_{ge}(0) = 1$, $A = 10$, $A_r = 0.8A_{gg}(1)$, $\eta = 0$ and $V = 0.5\,\mathrm{mV}$; (c) calculated nonlinear conductance for the same parameters as above, but strong power law relaxation rate: $\eta = 2$ and $A_r = 62.5A_{gg}(1)$. Other parameters and reference rate as in figure 3.

4. Results and comparison with experiment

4.1. Linear transport

Figure 3(c) shows the numerical results of the linear conductance for the transition $n \leftrightarrow n+1$. The trace in the (B, V_G)-plane reflects the position of the $n+1$-th energy level as a function of B. To obtain consistency with figure 2(b), we must assume that orbital effects influence the tunnelling more than spin effects, $A_{gg}(1) < A_s$, and that tunnelling discriminates between the two spin directions, $A_s < 1$, consistent with our above assumptions. The particular values chosen in figure 3(c) are $A_s = 0.3$ which yields the bimodal behaviour, and $A_{gg}(1) = A_s/5$, responsible for the reduced intensity of lines with positive slopes. The faint but still detectable lines with positive slopes imply $A_{gg}(1)/A_s < 1$ but not $\ll 1$. No information about $A_{ge}(q)$ can be obtained in the linear regime. Moreover, relaxation does not affect the linear transport and the barrier asymmetry yields only a global renormalization of the linear conductance. In the following, we fix A_s and $A_{gg}(1)$ to the values determined above.

4.2. Nonlinear transport

For $V > 0$ the $n \leftrightarrow n+1$ conductance trace splits (figure 4(a)). This yields 'stripes' in the (B, V_G)-plane defined by the traces corresponding to the transitions $n \to n+1$ and $n+1 \to n$. Between

these, new transitions involving excited states appear. However, the transitions corresponding to $n \to n+1$, which should appear at lower gate voltages, are not seen in the experiment (figure 2(d)). This allows us to estimate that $C_S/C_D \approx 0.1$. The traces at the higher gate voltages in figure 4(a) correspond to $g_{n+1} \to g_n$ and $g_{n+1} \to e_n$.

By varying A, $A_{ge}(q)$, A_r and η, many different behaviours of the conductance traces can be generated. We first discuss the case of constant relaxation, $\eta = 0$. Here, we found that the following hierarchy of parameters

$$A_{ge}(1) < A_{gg}(1) \approx A_r < A_s < A_{ge}(0), \tag{12}$$

supplemented by the condition on the barriers asymmetry $A>1$, leads to results in good agreement with the experimental findings, as can be seen in figure 4(b). In particular, we were able to reproduce the following features:

(i) a bimodal behaviour of NDC, PDC patterns for the negative-sloped traces corresponding to $g_{n+1} \to e_n$, and

(ii) the complete absence of traces corresponding to $g_{n+1} \to e_n$ with positive slopes.

Feature (i) is reproduced by imposing $A_r < A_s < A_{ge}(0)$ together with $A>1$. Specifically, $A_s<A_{ge}(0)$ ensures a spin-dependent alternating pattern of NDC and PDC lines. Tuning $A>1$ stabilizes even further NDC, inducing a dynamical trapping [17] of the excited states in the edge with n electrons. In order not to deplete NDC relaxation cannot exceed a critical threshold, therefore $A_r<A_s$ must be fulfilled.

Feature (ii) requires $A_{ge}(1)<A_{gg}(1) \approx A_r$. The first part of this condition implies that the timescale for tunnelling into an excited state in the core is much longer than the one for tunnelling into the corresponding ground state. Without relaxation, this would imply NDC in all excited state traces with positive slopes. However, by virtue of $A_{gg}(1) \approx A_r$, relaxation is sufficiently fast to detrap excited states in the core—yielding eventually a vanishing differential conductance—while still preserving dynamical trapping in the core. Figure 4(b) shows the result for $A_s = 0.3$, $A_{gg}(1) = A_s/5$, $A_{ge}(1) = A_{gg}(1)/9$, $A_{ge}(0) = 1$, $A = 10$, $A_r = 0.8A_{gg}(1)$ and $\eta = 0$.

Considering a power law dependence on the energy of the relaxation rate, $\eta > 0$, has important consequences on the results discussed above. In this case, condition (12) is replaced by

$$A_{ge}(1) < A_{gg}(1) \approx A_r(\Delta E/\omega_0)^\eta < A_s < A_{ge}(0), \tag{13}$$

where ΔE is the energy difference corresponding to the transition $e_n \to g_n$. Figure 4(c) shows the results for $\eta = 2$. It can be seen that the relaxation rate is less effective near the crossings of the lines $g_{n+1} \to g_n$ and $g_{n+1} \to e_n$: here NDC for excited states in the edge of the dot is more pronounced. Furthermore, lines with positive slope do not have anymore everywhere vanishing intensity, but show hints of NDC near the crossing points. Indeed, approaching the crossing points the energy difference ΔE tends to zero, thus $\gamma^r_{eg}(\Delta E) \to 0$—see equation (8)—and condition (13) is not satisfied. This, in turn, implies no de-trapping of the excited states in the core, signalled by a region of NDC in lines with positive slope. While for weak power laws ($\eta \lesssim 1$) the above effect is negligible, higher exponents lead to more pronounced effects.

4.3. Discussion

Here, we comment briefly on the role of interaction in view of the above relationships among tunnelling rates. The condition $A_{ge,gg}(1) < A_{ge,gg}(0)$ supports the idea that tunnelling into the core of the quantum dot is suppressed w.r.t. tunnelling into the edge. It is however hard to tell the influence of interactions by this observation since, already at the level of the tunnelling amplitudes, $|t^{\lambda}_{1\sigma}|^2 < |t^{\lambda}_{0\sigma}|^2$.

It has been suggested that in an interacting quantum dot, the ground-state-to-ground-state transitions have the largest transition probabilities [23], and transitions involving excited states are dominated by very few transition matrix elements between Slater states [24]. The rates involving excited states can therefore be smaller than those for the ground-state-to-ground-state transitions. Indeed, $A_{ge}(1) < A_{gg}(1)$ seems to confirm the above conclusion. However, such a strong condition is not mandatory for tunnelling rates involving states in the edge: $A_{ge}(0) \sim A_{gg}(0)$. Therefore it would be tempting to conclude that interactions in the core are stronger than in the edge of the dot.

The vanishing intensity of excited states lines with positive slope supports the idea that relaxation of the excited states is present, $A_{\mathrm{r}} > 0$. Without this mechanism, it would not be possible to explain why only excited states in the core get dynamically trapped. However, this mechanism seems sensitive to the specific type of relaxation process: while a good agreement with experimental data is possible for relaxation rates with a weak energy dependence, discrepancies are found around the crossing of conductance lines when strong power laws are considered.

5. Conclusion

In conclusion, we have compared measurements of the nonlinear conductance spectra of 2D quantum dots in a strong perpendicular magnetic field with current–voltage characteristics obtained by solving a master equation starting from a single-particle model. For reproducing qualitatively the most prominent experimental features in the nonlinear transport regime, it is not sufficient to assume spin-dependent tunnelling: we found optimum agreement when a specific hierarchy among rates is assumed and barriers asymmetry is taken into account. The mechanism we propose to explain the regular pattern of observed NDC/PDC along lines with negative slopes and the vanishing of conductance lines with positive slope relies on the dynamical trapping and de-trapping of excited states in the dot. This mechanism seems sensitive to the type of relaxation under consideration.

Acknowledgments

Financial support by the German BMBF, by the EU via contract MCRTN-CT2003-504574 and by the Italian MIUR via PRIN05 is acknowledged.

References

[1] Meirav U, Kastner M A and Wind S J 1990 *Phys. Rev. Lett.* **65** 771
[2] Kouwenhoven L P *et al* 1997 *Mesoscopic Electron Transport* vol 345 of Series E, ed G Schön (Dordrecht: Kluwer) pp 105–214
Reimann S M and Manninen M 2002 *Rev. Mod. Phys.* **74** 1283
Grabert H and Devoret M H (ed) 1991 *Single Charge Tunneling* (New York: Plenum) and references therein

[3] Kouwenhoven L P *et al* 2001 *Rep. Prog. Phys.* **64** 701
[4] Fock V 1928 *Z. Phys.* **47** 446
Darwin C G 1930 *Math. Proc. Camb. Phil. Soc.* **27** 86
[5] McEuen P L *et al* 1992 *Phys. Rev.* B **45** R11419
[6] Ciorga M *et al* 2000 *Phys. Rev.* B **61** R16315
[7] Ciorga M *et al* 2002 *Phys. Rev. Lett.* **88** 256804
[8] Rogge M C *et al* 2004 *Appl. Phys. Lett.* **85** 606
[9] Ciorga M *et al* 2002 *Appl. Phys. Lett.* **80** 2177
[10] Averin D V *et al* 1991 *Phys. Rev.* B **44** 6199
[11] Beenakker C W J 1991 *Phys. Rev.* B **44** 1646
[12] Yeyati A L *et al* 1999 *Phys. Rev. Lett.* **83** 600
[13] Thielmann A *et al* 2005 *Phys. Rev.* B **71** 045341
[14] Kießlich G *et al* 2003 *Phys. Rev.* B **68** 125320
[15] Weinmann D, Häusler W and Kramer B 1995 *Phys. Rev. Lett.* **74** 984
[16] Hüttel A K *et al* 2003 *Europhys. Lett.* **62** 712
[17] Cavaliere F *et al* 2004 *Phys. Rev. Lett.* **93** 036803
[18] Rogge M C *et al* 2003 *Appl. Phys. Lett.* **83** 1163
[19] Rogge M C *et al* 2004 *Physica* E **21** 483
[20] Sachrajda A S *et al* 2001 *Physica* E **10** 493
[21] Keller M *et al* 2001 *Phys. Rev.* B **64** 033302
[22] Khaetskii A V and Nazarov Yu V 2000 *Phys. Rev.* B **61** 12639
Bulaev D V and Loss D 2005 *Phys. Rev.* B **71** 205324
[23] Pfannkuche D and Ulloa S E 1995 *Phys. Rev. Lett.* **74** 1194
[24] Jauregui K *et al* 1996 *Phys. Rev.* B **53** R1713